Combined effects of Marangoni, sedimentation and coffee-ring flows on evaporative deposits of superparamagnetic colloids : Supplementary Materials

(Dated: July 29, 2019)

I. EVOLUTION OF MASTER CURVE PARAMETERS

This section presents and discusses the evolution of all the fit parameters of the master curve.

Fig. 1 shows the evolution of the parameters not described in the main text, regarding the Marangoni and Coffee-ring peak. (*a*) The parameter m_{Co} describes the dimensionless central position r/R of the coffee-ring peak. The distance from the centre of this peak is always close to 90% of the droplet radius and can be expressed as 0.9 ± 0.01 for all tested conditions. (*b*) The parameter σ_{Co} describes the standard deviation of the Gaussian modelling the coffee-ring peak in the deposit density. This standard deviation corresponds to a Full Width at Half Maximum $FWHM = 2\sqrt{2\ln(2)}\sigma_{Co}$ of $4.7\% \pm 1\%$ of the radius of the droplet for all tested conditions. (*c*) The parameter m_{Ma} describes the dimensionless central position r/R of the Marangoni eddy. One can see that this peak is always closer to the centre of the droplet than the coffee-ring peak, often near $r/R = 0.7 \pm 0.1$. However, there are two points where this position drops near 0 (for $\kappa_0 = 50.\,10^{-3}$, $B = 13.5\,10^{-4}\,\mathrm{T}$ and $B = 22.5\,10^{-4}\,\mathrm{T}$). In this case, the best Marangoni eddy is fitted in the centre of the droplet, meaning that such a peak, if it still exists, is lost in the data's noise. Accordingly, as one can see in Fig. 3 of the main text, the amplitude of the Marangoni peak in these cases is pretty low. We kept the points of Ma for these cases as an estimation of the maximal value of the amplitude of the Marangoni eddy. (*d*) The parameter σ_{Ma} describes the standard deviation of the Gaussian modelling the coffee-ring peak in the deposit density. This standard deviation corresponds to a Full Width at Half Maximum $FWHM = 2\sqrt{2\ln(2)}\sigma_{Ma}$ of $20\% \pm 10\%$ of the radius of the droplet for all tested conditions, except for $\kappa_0 = 50.\,10^{-3}$, $B = 13.5\,10^{-4}\,\mathrm{T}$ and $B = 22.5\,10^{-4}\,\mathrm{T}$. For the first point, the width of the peak is close to 0, meaning that the fitted peak is actually a small fluctuation in the homogeneous background. For the second point, the peak is larger than usual, meaning that the fitted peak is lost in a larger part of the homogeneous background. This is due to the trend of the Marangoni peak to vanish for high PBS concentration and magnetic field.

II. MAGNITUDE ORDERS

To understand the evolution of the different parameters from Eq. (4) of the main text, it is useful to compare the characteristic speed of each mechanism occuring in our system. In the magnitude order considerations which follow, we take all the values in SI units and therefore do not always recall the units, in order to avoid overloading the equations.

A. Mass conservation flow

Typical speed of the coffee-ring effect v_{CR}, induced by the flow of mass conservation, solely depends on the geometry of the droplet and scales as

$$v_{CR} \sim \frac{h_0\ R}{h\ t_f}, \tag{1}$$

where h is the height of the droplet, h_0 is the initial height, R is the radius droplet and t_f is the time required to completely evaporate the drop [1, 2]. It is then time-dependent and diverges near the end of the evaporation, but it is worthwhile to notice that it does not depend on the varied parameters of our experiments, B and κ_0. The characteristic value of this speed at the beginning of the evaporation (for a droplet of height $h_0 \sim 10^{-3}\,\mathrm{m}$, radius $R \sim 10^{-3}\,\mathrm{m}$ and an evaporation time of $10^3\,\mathrm{s}$) has a magnitude scaling as $v_{CR} \sim 10^{-6}\,\mathrm{m/s}$.

B. Marangoni recirculation speed

Typical speed of Marangoni recirculation v_{Ma} scales as

$$v_{Mg} \sim \frac{\mathrm{Mg}h}{t_f} \tag{2}$$

where Mg is the Marangoni number

$$\mathrm{Mg} = (\frac{\partial\gamma}{\partial\kappa}\ \kappa_0\ t_f)/(\eta\ R), \tag{3}$$

where γ is the surface tension, and η the viscosity of the liquid [1, 2]. We can then write

$$v_{Mg} \sim \frac{\partial\gamma}{\partial\kappa}\ \frac{\triangle\kappa\ t_f h_0}{\eta\ R t_f} \sim 10^{-1}\kappa_0\,\mathrm{m/s} \tag{4}$$

as the characteristic value of the Marangoni recirculation speed, since $\eta \sim 10^{-3}\,\mathrm{Pa\ s}$ and $\frac{\partial\gamma}{\partial\kappa} \sim 10^{-4}\,\mathrm{N/m^2}$ [3].

C. Sedimentation speed

Since we can consider we are in a viscous regime, the characteristic speed of sedimentation v_S depends on DLVO forces F_{DLVO}, the effective weight of the agglomerates W (taking into account both gravity and buoyancy) and the drag coefficient of the agglomerates

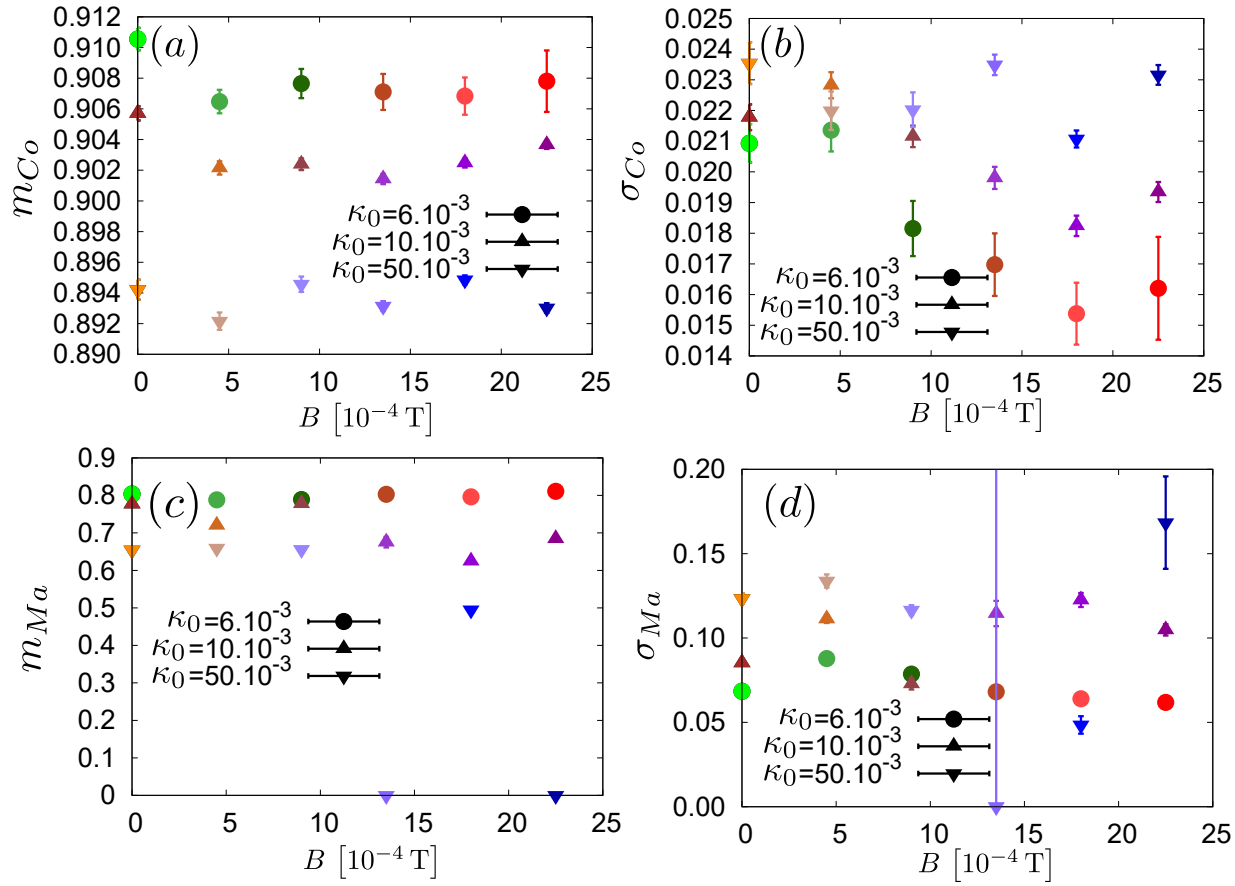

FIG. 1. Fit parameters from the master curves. (a) The parameter m_{Co} describes the dimensionless central position r/R of the coffee-ring peak. (b) The parameter σ_{Co} describes the standard deviation of the Gaussian modelling the coffee-ring peak in the deposit density. (c) The parameter m_{Ma} describes the dimensionless central position r/R of the Marangoni eddy. (d) The parameter σ_{Ma} describes the standard deviation of the Gaussian modelling the coffee-ring peak in the deposit density.

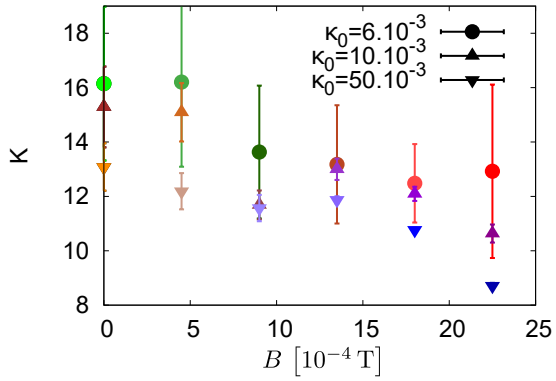

FIG. 2. Evolution of the K parameter of the fitted curves. One can see that this parameter is mainly constant and around 13 ± 3.

$D \propto \eta a$, where η is the viscosity of the fluid and a the typical size of the agglomerates (we define here the drag coefficient as the ratio between the drag force and the relative speed of the object in the fluid). We then have $v_S \propto (F_{DLVO} + W)/D$.

1. *DLVO forces*

The DLVO forces are the sum of electrostatic repulsion F_e and van der Waals attraction F_{VdW} : $F_{DLVO} = F_e + F_{VdW}$. If we note λ the Debye screening length, the electrostatic repulsion F_e between particles and the substrate, taking into account the double layer of ions, scales as

$$F_e \sim -64\pi d n k_B T \lambda \exp(z/\lambda) \tag{5}$$

where n is the number of counterions per unit volume (molecules by m^3), z is the interdistance between the substrate and the particle, k_B is the Boltzmann constant, T the temperature and d is the particle's diameter. In order to assess a typical magnitude for this force, let us first estimate the Debye length λ

$$\lambda \sim \sqrt{\frac{\epsilon_r \epsilon_0 k_B T}{2 N_A e^2 I}} \sim \frac{\lambda_{PBS}}{\sqrt{\kappa_0}} \sim \frac{10^{-9}}{\sqrt{\kappa_0}} \text{ m}, \tag{6}$$

where $\epsilon_r \epsilon_0$ is the effective electric permittivity of water, N_A is the Avogadro number, e the fundamental charge of the electron and $I = \kappa_0 I(PBS)$ the ionic strength of the

dispersant ($I(PBS)$ is the ionic strength of pure PBS) [4, 5]. All of those constant can be expressed in terms of the Debye length of pure PBS, $\lambda_{PBS} \sim 10^{-9}$m [5], and the dilution of PBS, κ_0. We can also assess the number of counterions n

$$n \sim N_A\, 10^3 \kappa_0 C_{PBS} \sim 10^{25}\, \kappa_0 \text{ m}^{-3}, \tag{7}$$

since the concentration C_{PBS} of ions in PBS is dominated by the concentration of NaCl and then $C_{PBS} \approx$ 137mmol/L ~ 0.1 M. Taking into account those two estimations, we eventually obtain that the electrostatic repulsion, assessed at the Debye length, goes like $F_e \sim 10^{-9}\sqrt{\kappa_0}$ N. All in all, we obtain a characteristic value for the electrostatic force $F_e \sim 10^{-9}\sqrt{\kappa_0} \sim 10^{-10}$ N, given the range of $\kappa_0 \in [6\,10^{-3}, 5\,10^{-2}]$ we explored. The van der Waals interaction forces, estimated at the Debye length, scale as

$$F_{VdW} \sim \frac{Ad}{\lambda^2} \sim 10^{-8}\kappa_0 \text{ N}, \tag{8}$$

where A is the Hamaker constant, $A = 2.43\,10^{-20}$ J for water. In our case, the van der Waals interaction then goes from 10^{-11} N to 10^{-10} N. We can already conclude that we will have a transition in our system. Indeed, for low PBS concentration $\kappa_0 = 6\ 10^{-3}$ we have $F_{VdW} < F_e$ while, for high concentration $\kappa_0 = 50\ 10^{-3}$, we have $F_{VdW} \approx F_e$. In the former case, the complete sedimentation will be at least slowed down thanks to electrostatic repulsion, while for the latter van der Waals interactions are likely to create a faster sedimentation. We will show here that this can explain the behavior of the curves in Fig. (3) of the main text.

2. Agglomerates properties

Before discussing the curves in Fig. (3) of the main text, we still have to assess the weight W of each agglomerates and their drag coefficient D. First of all, let us notice that the typical length of those agglomerates grows like

$$\langle L \rangle \sim d\left(1 + \frac{\phi\chi^2 t_f B^2}{\eta\mu_0}\right)^{0.65} \sim 10^{-6} + 0.1\, B^{1.3} \text{ m}, \tag{9}$$

where $\phi \sim 10^{-3}$ is the volume fraction of the colloidal particles, $\chi \sim 0.1$ is their magnetic susceptibility and $\mu_0 \approx 4\pi\, 10^{-7}$ is the magnetic permeability of water[3]. Given the magnetic field B goes from 0 to 10^{-3} in our experiments, this length ranges from 10^{-6} to 10^{-5}. From this we can compute the drag coefficient [6]

$$D \approx \frac{\eta\langle L \rangle}{\ln \frac{\langle L \rangle}{d} - 0.5} \sim \eta\langle L \rangle \sim 10^{-9} + 10^{-4}\, B^{1.3} \text{ kg/s}, \tag{10}$$

from which we can infer that the drag coefficient D goes from 10^{-9} kg/s to 10^{-8} kg/s. The effective weight of each agglomerate can be assessed as

$$W \sim \delta g \langle L \rangle d^2 \sim 10^{-14} + 10^{-9} B^{1.3} \text{ N}, \tag{11}$$

where $\delta \sim 10^3$ kg/m^3 is the difference in the volume density between the particles and the water and $g \sim 10$ m/s^2 is the gravitational acceleration. From previous range for B, we then infer that this force is comprised between 10^{-14} N and 10^{-13} N.

3. Global sedimentation speed

We can then distinguish two regimes regarding the sedimentation speed, depending on the concentration of PBS in the droplet. If the PBS concentration is small enough $\kappa_0 \sim 10^{-3}$, then the DLVO forces repel the particles from the substrate when they are close enough (typically at the Debye length). The only characteristic sedimentation speed is then the one obtained in the bulk of the droplet and determined by the effective weight of the particles : $v_S = W/D \sim 10^{-5}$ m/s. In this case, we then have $v_{CR} \sim 10^{-6}$ m/s $<<$ $v_S \sim 10^{-5}$ m/s $<<$ $v_{\text{Mg}} \sim 10^{-4}$ m/s. If the concentration of PBS is high enough, the DLVO forces between the particles and the substrate become attractive and the sedimentation is also characterized by the force which makes the particles stick to the substrate. The speed associated with this motion can be assessed as $v_S \approx F_{DLVO}/D$. In this case, since we are close to the transition, we can estimate that the DLVO forces are at least of the order of 10% of the electrostatic and van der Waals forces : $F_{DLVO} \sim 10^{-11}$ N. In this case, the sedimentation speed range is $v_S \sim 10^{-2}$ m/s for each individual particles. We then have $v_{CR} \sim 10^{-6}$ m/s $<<$ $v_{\text{Mg}} \sim 10^{-3}$ m/s $<<$ $v_S \sim 10^{-2}$ m/s.

D. Evolution of the density profile parameters

If we assume

$$Co \propto (v_{CR} - v_S - v_{Mg})/(Co + C + Ma), \tag{12}$$
$$C \propto (v_S + v_{Mg} - v_{CR})/(Co + C + Ma) \tag{13}$$
$$\text{and } Ma \propto (v_{Mg} - v_S - v_{CR})/(Co + C + Ma), \tag{14}$$

the different behaviours in our system can be understood by comparing the three characteristic speeds. These hypotheses come from the fact that if the sedimentation makes the particles stick to the substrate, the fluid will not be able to move them at its own velocity, but will have to act against the sedimentation forces through a drag force. Moreover, the Marangoni speed and the coffee-ring speed simply add up to determine the actual flow in the droplet [1]. Then the effective speed for Coffee-ring construction $v_{eff,Co}$ verifies $D\, v_{eff,Co} = D\,(v_{CR} - v_{Mg}) - D\, v_S \Leftrightarrow v_{eff,Co} = v_{CR} - v_{Mg} - v_S$. The same reasoning holds for the Marangoni eddy construction $v_{eff,\text{Ma}} = v_{Mg} - v_{CR} - v_S$.

For high values of κ_0, for a given magnetic field B, v_S and v_{Mg} will increase while $v_C R$ will remain constant. This explains the vertical shifts of the curves in Fig. (3) of the main text for increasing values of κ_0. Moreover,

we obtained in those case $v_{CR} \sim 10^{-6}$ m/s $<< v_{\rm Mg} \sim 10^{-3}$ m/s $<< v_S \sim 10^{-2}$ m/s for particles close to the substrate. The coefficients Ma and Co will then be fixed by the sedimentation speed v_S. However, the order of magnitude of the various speeds is only true when particles are close to the substrate. One can understand that bulk sedimentation speed still determines the number of particles reaching the substrate and then Ma, Co and C still depend on the magnetic field through the bulk sedimentation speed $v_S \propto \frac{10^{-14}+10^{-9}B^{1.3}}{10^{-9}+10^{-4}B^{1.3}}$. Then, the coefficient $C \propto (v_S + v_{\rm Mg})/(Co + C + Ma)$ will grow with B while Co and Ma will substantially decrease. When $C >> Co, Ma$, given the normalization of those parameters, all parameters should saturate when C approaches 1. More accurately, one can determine the dominating terms in B and κ_0 in the previous terms. One obtains the scaling

$$Co \propto \frac{\alpha_1 + \alpha_2 B^{1.3} + \alpha_3 \kappa_0}{\alpha_4 + \alpha_5 B^{1.3} + \alpha_6 \kappa_0} \tag{15}$$

$$C \propto \frac{\beta_1 + \beta_2 B^{1.3} + \beta_3 \kappa_0}{\beta_4 + \beta_5 B^{1.3} + \beta_6 \kappa_0} \tag{16}$$

$$\text{and } Ma \propto \frac{\zeta_1 + \zeta_2 B^{1.3} + \zeta_3 \kappa_0}{\zeta_4 + \zeta_5 B^{1.3} + \zeta_6 \kappa_0} \tag{17}$$

where $\alpha_i, \beta_i, \zeta_i > 0$ are fitting parameters. One also expects $\alpha_1 \sim \alpha_2\, 10^{-5} \sim \alpha_4 \sim \alpha_5\, 10^{-5}$, and alike for the corresponding β and ζ coefficients. Indeed, those various terms come from the same characteristic sedimentation speed v_S. Fits of the corresponding trends, respecting the aforementioned relations for the fitting coefficients α_i, β_i and ζ_i are represented on Fig. 3 of the main text and explains the trend of the data in this Figure.

In the case of low initial PBS concentration κ_0, we established that we have $v_{CR} \sim 10^{-6}$ m/s $<< v_S \sim 10^{-5}$ m/s $<< v_{\rm Mg} \sim 10^{-4}$ m/s. Particles can then not completely sediment on the substrate and only the Marangoni speed $v_{\rm Mg}$ is relevant in this case. It is worthwhile to notice that the bulk sedimentation speed v_S still increases with B since $W/D \propto \frac{10^{-14}+10^{-9}B^{1.3}}{10^{-9}+10^{-4}B^{1.3}}$. In this case, Co will decrease with B, while C and Ma can stay more or less constant. Indeed, given $Co << Ma, C$ and $v_S << v_{\rm Mg}$, we have $C \propto v_{\rm Mg}/(C + Ma)$ and $Ma \propto v_{\rm Mg}/(C + Ma)$. More accurately, one can determine the dominating terms in B and κ_0 in the previous terms. The dominating term in κ_0 goes like $\sqrt{\kappa_0}$. We can then consider the evolution of C,Co and Ma separately for this concentration. One then obtains the scaling

$$Co \propto \frac{\alpha'_1 + \alpha'_2 B^{1.3}}{\alpha'_4 + \alpha'_5 B^{1.3}} \tag{18}$$

$$C \propto \frac{\beta'_1 + \beta'_2 B^{1.3}}{\beta'_4 + \beta'_5 B^{1.3}} \tag{19}$$

$$\text{and } Ma \propto \frac{\zeta'_1 + \zeta'_2 B^{1.3}}{\zeta'_4 + \zeta'_5 B^{1.3}} \tag{20}$$

with the same constraints regarding the prime parameters. Those curves are represented on Fig. 3 of the main text.

[1] Hu, H. & Larson, R. G. Marangoni effect reverses coffeering depositions. *The Journal of Physical Chemistry B* **110**, 7090–7094 (2006).

[2] Darras, A., Vandewalle, N. & Lumay, G. Transitional bulk-solutal marangoni instability in sessile drops. *Physical Review E* **98**, 062609 (2018).

[3] Darras, A., Mignolet, F., Vandewalle, N. & Lumay, G. Remote-controlled deposit of superparamagnetic colloidal droplets. *Physical Review E* **98**, 062608 (2018).

[4] Bhardwaj, R., Fang, X., Somasundaran, P. & Attinger, D. Self-assembly of colloidal particles from evaporating droplets: role of dlvo interactions and proposition of a phase diagram. *Langmuir* **26**, 7833–7842 (2010).

[5] Sultan, S., de Planque, M., Ashburn, P. & Chong, H. Effect of phosphate buffered saline solutions on top-down fabricated zno nanowire field effect transistor. *Journal of Nanomaterials* **2017** (2017).

[6] Promislow, J. H., Gast, A. P. & Fermigier, M. Aggregation kinetics of paramagnetic colloidal particles. *J. Chem. Phys.* **102**, 5492–5498 (1995).